Published in final edited form as:
J Comp Neurol. 2009 September 10; 516(2): 94–104. doi:10.1002/cne.22093.

Blood Vessels Form a Migratory Scaffold in the Rostral Migratory Stream

Mary C. Whitman, **Wen Fan**, **Lorena Rela**, **Diego J. Rodriguez-Gil**, and **Charles A. Greer**
Yale University School of Medicine Departments of Neurobiology and Neurosurgery New Haven, CT 06511

Abstract

In adult mice, new neurons born in the subventricular zone (SVZ), lining the lateral ventricles, migrate tangentially into the olfactory bulb along a well-delineated path, the Rostral Migratory Stream (RMS). Neuroblasts in the RMS migrate tangentially in chains, without a recognized migratory scaffold. Here, we quantitatively examine the distribution of, and relationships between, cells within the RMS, throughout its rostral-caudal extent. We show that there is a higher density of blood vessels in the RMS than in other brain regions, including areas with equal cell density, and that the orientation of blood vessels parallels the RMS throughout the caudal to rostral path. Of particular interest, migratory neuroblast chains are longitudinally aligned along blood vessels within the RMS, with over 80% of vessel length in rostral areas of the RMS apposed by neuroblasts. Electron micrographs show direct contact between endothelial cells and neuroblasts, although intervening astrocytic processes are often present. Within the RMS, astrocytes arborize extensively, extending long processes which are parallel to blood vessels and the direction of neuroblast migration. Thus, the astrocytic processes establish a longitudinal alignment within the RMS, rather than a more typical stellate shape. This complementary alignment suggests that blood vessels and astrocytes may cooperatively establish a scaffold for migrating neuroblasts, as well as provide and regulate migratory cues.

Keywords

Neuroblast migration; olfactory bulb; subventricular zone; glia; mouse; adult neurogenesis; astrocyte; endothelium

INTRODUCTION

In adult mammals, neurogenesis in the subventricular zone (SVZ) lining the lateral ventricles generates neuroblasts that migrate significant distances into the olfactory bulb (OB) via a well-delineated path, the Rostral Migratory Stream (RMS) (Lois and Alvarez-Buylla, 1994). In the SVZ, glial fibrillary acidic protein (GFAP)-expressing stem cells divide, forming transit amplifying cells which divide rapidly to generate up to 30,000 neuroblasts daily (Alvarez-Buylla et al., 2001; Doetsch et al., 1999). The neuroblasts coalesce into densely packed chains as they enter the RMS (Doetsch and Alvarez-Buylla, 1996; Jankovski and Sotelo, 1996). Throughout the adult RMS, chains of neuroblasts remain associated with $GFAP^+$ astrocytes; in the embryonic RMS $GFAP^+$ astrocytes do not appear until E16, 2-3 days following the initial formation of the RMS (Pencea and Luskin, 2003). Upon reaching the OB, the chains dissociate and neuroblasts migrate radially into the

Corresponding Author: Charles A. Greer, Ph.D. Department of Neurosurgery Yale University School of Medicine P.O. Box 208082 New Haven, CT 06520-8082 Telephone – 203.785.4034 charles.greer@yale.edu.

granule cell layer (GCL) or glomerular layer (GL), where they differentiate into granule or periglomerular cells, respectively (Whitman and Greer, 2007a; Whitman and Greer, 2007b).

The relationship between migrating neuroblasts and surrounding glia in the RMS is complex. In adults, astrocytes surround neuroblasts, forming glial tubes that may establish boundaries within which neuroblasts migrate (Alvarez-Buylla and Garcia-Verdugo, 2002; Lois and Alvarez-Buylla, 1994; Lois et al., 1996). These glial boundaries may physically restrict neuroblast migration, preventing premature exit from the RMS, and may also provide directional cues for migrating neuroblasts (Ghashghaei et al., 2007). *In vitro*, astrocytes are not required for chain formation (Wichterle et al., 1997), but the loss of any of several molecules expressed by migrating neuroblasts, including β1integrin (Belvindrah et al., 2007), ErbB4 (Anton et al., 2004), and NCAM (Chazal et al., 2000), disrupts both RMS glial processes and neuroblast migration. SVZ and RMS astrocytes also modulate the microenvironment, regulating GABA and glutamate levels, which in turn modulate neuroblast migration speed (Bolteus and Bordey, 2004; Platel et al., 2007).

Endothelial cells may also play a role in the maturation and migration of adult-born neuroblasts; in the embryo, neurogenesis and angiogenesis are often stimulated by the same growth factors (Carmeliet and Tessier-Lavigne, 2005; Klagsbrun and Eichmann, 2005; Ward and Lamanna, 2004). In the SVZ, blood vessels form a vascular niche for neural stem cells (Alvarez-Buylla and Lim, 2004; Tavazoie et al., 2008). In stroke models, neuroblasts migrate from the SVZ to the area of infarct closely apposed to blood vessels (Ohab et al., 2006; Thored et al., 2007; Yamashita et al., 2006), perhaps due to vascular production of angiopoietin 1 (Ang1) and stromal-derived factor 1 (SDF1) (Ohab et al., 2006). Recent evidence also found neuroblasts in the OB were associated with blood vessels (Bovetti et al., 2007).

A unique aspect of migration in the RMS is the apparent absence of a migratory scaffold. Here, we show blood vessels are aligned parallel to the path of migration within the RMS and are closely apposed by chains of migratory neuroblasts. The complementary parallel alignment of $GFAP^+$ processes suggests that both blood vessels and astrocytes may cooperatively establish an RMS scaffold, around which migrating neuroblasts are organized.

EXPERIMENTAL METHODS

Animals

C57BL6 male mice, 12 - 14 wk old, (Charles River Laboratories) were housed in groups of 3 with a 12 hr light/dark cycle and access to food and water *ad libitum*. All animal care and use was approved by the Yale University Animal Care and Use Committee. Processing of mice and related procedures generally followed those we have previously described (Whitman and Greer, 2007a; Whitman and Greer, 2007b). Mice were anesthetized with pentobarbital and perfused transcardially with PBS with 1 unit/ml heparin, followed by 4% paraformaldehyde. The brain was removed from the skull and post-fixed in the same fixative for two hrs. Brains were rinsed in PBS overnight, cryo-preserved in 30% sucrose in PBS, cut on a sliding-freezing microtome (50μm), and stored at −20°C until use.

For electron microscopy, the mice were perfused with 4% paraformaldehyde and 2% glutaraldehyde, followed by post-fixation in the same fixative for 4 hrs. Brains were rinsed in PBS overnight, and cut on a vibratome (50μm).

DCX-EGFP mice (GENSAT BAC transgenic, strain name STOCK Tg(Dcx-EGFP)1Gsat/Mmmh) were a kind gift of Dr. Angelique Bordey. They were originally made by injecting multiple copies of a BAC containing EGFP upstream of the coding sequence of DCX into

the pronuclei of FVB/N fertilized oocytes. Hemizygous progeny were then mated to Swiss Webster mice (Gong et al., 2003). For dye injections, 6 DCX-EGFP mice, 5-6 weeks of age, were treated as above, except OBs were postfixed for 6 hrs, washed with 0.1 M PB (pH 7.4) and sliced on a vibratome (300 μm) in the coronal, horizontal or sagittal plane. Slices were stored in 0.1 M PB (pH 7.4) at 4°C for up to 10 days and were stained with DAPI before use.

Immunohistochemistry

Tissue was warmed to room temperature (RT), then washed in PBS with 0.3% Triton X-100 (PBS-T) for 10 min at RT. Tissue was blocked with 2% BSA in PBS-T at RT for 30 min and incubated with primary antibodies diluted in blocking buffer at 4°C overnight. Sections were washed with PBS-T, incubated in secondary antibodies, DAPI (nuclear marker, Invitrogen) and DRAQ5 (nuclear marker, Alexis Biochemicals, San Diego, CA) for 2 hrs at RT, washed in PBS-T, then PBS, and mounted in GelMount (Biomeda, Foster City, CA).

Primary Antibodies and Concentrations—goat anti-doublecortin (DCX), 1:1000 The polyclonal goat-antidoublecortin (DCX) antibody was raised against a synthetic peptide corresponding to amino acids 385-402 at the C-terminus of human doublecortin (Santa Cruz Biotechnology, Santa Cruz, CA; catalog No. sc-8066). Western blotting with this antibody detects a single band of 40 kDa molecular weight (Brown et al., 2003). Immunostaining with DCX stained the expected population of cells, consistent with published results (Komitova et al., 2009) and with the pattern seen in the DCX-GFP transgenic mouse.

Mouse anti-glial fibrillary acidic protein (GFAP)-cy3, 1:1000 The mouse monoclonal anti-glial fibrillary acidic protein (GFAP) antibody was raised against purified GFAP from pig spinal cord (Sigma-Aldrich, St. Louis, MO; catalog No. C9205, clone G-A-5, lot No. 103K4850). The antibody specifically localizes GFAP in immunoblotting assays (manufacturer's technical information) and stained cells with the classic morphology of astrocytes, consistent with published results (Komitova et al., 2009).

Rabbit anti-platelet endothelial cell adhesion molecule (PECAM), 1:500; a gift from Dr. J. Madri. This antibody was produced as described by immunizing rabbits with a recombinant protein containing the 6 IgG domains of PECAM (CD31) (amino acids 1-573), produced by a cell line provided by Dr. Beat Imhof (Piali et al., 1995). Western blots show a single band of the expected molecular weight, PECAM can be specifically immunoprecipitated, and tissue sections show the expected staining throughout the vasculature, during development (Pinter et al., 1997; Pinter et al., 1999). In our study, the antibody specifically localized to the vasculature.

Secondary Antibodies and Concentrations—donkey anti-goat-Alexa 488 1:1000 (Invitrogen); donkey anti-rabbit-Alexa 555 1:1000 (Invitrogen); donkey anti-goat-Cy5 1:1000 (Jackson); donkey anti-rabbit-Alexa 488 1:1000 (Invitrogen) donkey anti-guinea pig-Cy2 1:1000 (Jackson).

Electron Microscopy

Vibratome sections were stained with osmium tetroxide and embedded for thin sectioning in EPON. Sections of 70-100 nm were examined on a JEOL transmission electron microscope and photographed at primary magnifications of 4,000 – 8,000X.

Image Acquisition and Analysis

Images were acquired using a Leica confocal microscope as either Z-stacks taken through the full thickness of the RMS, with 1.0 μm steps between optical sections, or as single

optical planes. A minimum of five sagittal sections or ten coronal sections per animal were imaged and analyzed for each set of measurements. Sections were chosen based on the presence of RMS, which was delineated based on DCX^+ staining and the high density of nuclei. Digitized images were analyzed using Metamorph software (Molecular Devices, Sunnyvale, CA). Data were collected on individual optical sections. Levels were adjusted in Adobe Photoshop but images are otherwise unaltered.

Determination of Locations Along the RMS

Using sagittal sections, five areas along the RMS were selected, similar to (Pencea and Luskin, 2003) (Figure 1A): SVZ, along the lateral ventricles; Descent, along the descending portion of the RMS; Elbow, the ventral-most portion of the RMS; Enter, where the RMS enters the OB; and In Bulb. In coronal sections (Figure 1C), these were confirmed visually by: first occurrence of the lateral ventricles (SVZ); long dorsal-ventral extension of the RMS (Descent); most ventral RMS (Elbow); visible granule cell layer only in medial sections of OB (Enter); and oblong OB shape (in Bulb).

Quantitative Analysis

Cell Density—Freeform regions were drawn surrounding the RMS on coronal images. Labeled cells were counted using the Manual Count feature of Metamorph software on individual optical sections. Counted sections were spaced at least 20 um apart. All DCX+ and DCX− nuclei greater than 3 um in diameter with more than 50% of the nucleus within the region were counted. Adjacent optical sections were used to confirm DCX labeling. Counts were corrected using the Abercrombie correction factor (T/(T+h)), where T is the thickness of the optical section (1.02 μm), and h is the height (z-dimension) of the nuclei (7.17 μm in the RMS, and 5.71 μm in the cerebellum).

Blood Vessel Density—Freeform regions were drawn surrounding the RMS on sagittal images. Regions were also drawn around the granule cell layer of the cerebellum. Images were thresholded for the PECAM channel by eye. Using Metamorph software, the percentage of each region filled with PECAM staining was determined. Measurements for regions in and out of the RMS were done on the same images, with the same thresholds. Because the cross-sectional diameter of the blood vessels identified with PECAM staining did not differ in the regions studied, correction factors were not required. The quantification shown was done on sagittal sections, but we repeated the measurement on coronal sections and found the same pattern, indicating that the increased density seen is not an artifact of vessel orientation.

Blood Vessel Linear Apposition Percentage—In sagittal images, longitudinally cut blood vessels over 50 μm in length were measured for total length and length with DCX^+ cells directly apposed to the vessel. Each vessel was counted only once, even if it appeared in multiple optical sections.

Glial Process Density—On coronal images, non-overlapping 9.5 μm diameter circles were drawn within the RMS and in the immediate vicinity (within one cell body distance) surrounding the RMS. Region locations were randomly chosen with the GFAP channel turned off. Images were thresholded by eye. Since GFAP stains processes better than cell bodies, and we were more interested in total area of glial processes, rather than number of glial cells, we used relative optical density (area above threshold) to compare the density of processes in different regions, rather than counting cell bodies. Measurements of optical density in and around the RMS were conducted on the same images, with the same thresholds.

Statistical Analysis

For blood vessel density and glial process density, measurements were normalized to the mean value for each animal, giving a relative index for each animal that was subsequently used in statistical analyses. One or two-way ANOVAs, followed by posthoc t-tests (Bonferroni's Multiple Comparison test and Bonferroni posttests, respectively), were used to test for differences between locations along RMS and, where applicable, in versus out of RMS. Levels of significance were $p<0.05$.

Dye Injections

For dye injections, borosilicate glass (Sutter Instrument, Novato, CA) micropipettes with an impedance of 100-200 MΩ were filled with a 4% solution of Microruby, a 3000 kDa rhodamine-biotin-conjugated dextran (Invitrogen Molecular Probes, Carlsbad, CA) dissolved in 50 mM Tris-HCl (pH 7.4). The slices were transferred to an injection chamber containing 0.1 M PB (pH 7.4) and secured with a slice hold-down (Warner Instruments, Hamden, CT).

The slices were observed under an Olympus BX51 microscope with a water immersion objective and illuminated with a Lambda LS xenon lamp (Sutter Instrument, Novato, CA). The RMS was identified by the GFP fluorescence of migrating neuroblasts. DAPI staining provided a visual target to guide the dye-filled pipette. RMS astrocytes were chosen based on the location of their nuclei in the RMS and their lack of GFP fluorescence. The dextran conjugate was iontophoretically injected into the cell bodies of target cells by applying 500-msec current pulses (1-5 nA) at 1 Hz, during 15 min. The stimulus was delivered with a Multiclamp 700B amplifier and controlled with pClamp 10 software via a Digidata 1440A digitizer (Molecular Devices, Union City, CA). Injected slices were postfixed with 4% PFA for 24-48 hours at 4°C, washed with 0.1 M PB, stained with DRAQ5, mounted with GelMount and scanned with a Leica confocal microscope, using the 63X objective and 0.25 – 0.5 μm steps between optical sections. The morphology of the injected cells was reconstructed with Imaris software (Bitplane, Saint Paul, MN), and is displayed as volume reconstructions. When immunohistochemistry was performed after fixation of the filled cells, the dextran signal was amplified using streptavidin conjugated to Alexa Fluor 555 (2 mg/ml, Molecular Probes).

RESULTS

Although the path of migration from the SVZ to the OB in mice is several millimeters long, most studies of migration in the adult RMS have not distinguished between different locations along the RMS (cf. Pencea and Luskin, 2003). To study how migration and morphology might change along the caudal to rostral path of the RMS, we first divided the RMS into five regions (Figure 1A): 1) *SVZ*, the region adjacent and slightly rostral to the lateral ventricles; 2) *Descent*, where the RMS turns ventrally; 3) *Elbow*, the most ventral region of the RMS in the olfactory peduncle; 4) *Enter*, where chains of migrating neuroblasts first come into the OB; and 5) *In Bulb*, the continuation of the migratory stream within the OB, sometimes referred to as the subependymal layer of the OB. We defined the RMS by the presence of doublecortin (DCX)-expressing cells and the markedly increased cell density relative to surrounding regions. Divisions were originally defined in sagittal sections, and confirmed with landmarks in coronal sections.

We measured the overall cell density and density of DCX^+ neuroblasts in each region. As shown in Figure 1B, throughout the RMS the cell density is high, over 1.7 million cells/mm^3, and both overall and DCX^+ densities increase significantly in the Elbow, as the RMS reaches its ventral-most and narrowest point in the olfactory peduncle (overall: one-way

ANOVA, $p<0.0003$, Bonferroni's post-test Elbow significantly different from all other regions, $p<0.05$; DCX: one-way ANOVA, $p<0.0018$, Bonferroni's post-test Elbow significantly different from all other regions, $p<0.05$). The cross-sectional area of the RMS in the Elbow appears smaller (Figure 1D), thus the increased density likely reflects an equivalent number of cells transiting through a smaller space, and not an absolute increase in the number of cells. However, the overall increase in density within the elbow is accounted for solely by the increase in DCX^+ density, as there is no significant difference in the density of DCX^- cells. The stability of DCX^- density in different regions of the RMS suggests that the density of non-migratory cells in the RMS is not dependent on the density of neuroblasts and that structural elements do not change along the course of the RMS. The proportion of DCX^+ cells in the RMS increased from the SVZ (61.1±4.5%) to the bulb entrance (76.7± 2.3%) before decreasing slightly within the bulb (71.5±3.6%) (Figure 1C, $p<0.05$). The increase may reflect the maturation of precursor and transit amplifying cells in the caudal regions of the RMS into DCX^+ neuroblasts as they migrate rostrally.

Throughout the RMS, it was evident that chains of migrating cells were often closely associated with blood vessels, which appeared parallel to the caudal to rostral orientation of the RMS. To further investigate the association of blood vessels and neuroblasts in the RMS, we labeled blood vessels using an antibody to Platelet-Endothelial Cell Adhesion Molecule (PECAM; CD31), which is endothelial cell specific (Pinter et al., 1997).

It was immediately apparent that $PECAM^+$ blood vessels within the RMS are largely aligned parallel to the direction of RMS migration (Figure 2). In contrast, blood vessels outside the RMS, but in close proximity, or in areas of otherwise similar cell density, such as the cerebellum, are random in orientation (Figure 2A,I). Chains of DCX^+ neuroblasts are found directly apposed to blood vessels, often for long distances that can exceed 300 μm in single micrographs. This is most clearly seen within the OB, as the chains become less densely packed and individual migrating chains are easier to visualize (Figure 2D,E). In addition to the parallel alignment, there appeared to be a higher density of blood vessels within the RMS. To quantify this, we compared PECAM staining within the RMS to surrounding areas, and found that in all areas, blood vessel density was higher within the RMS. The quantification shown in Figure 2J was done on sagittal sections, but the pattern was the same on coronal sections, indicating that the increased density seen is not an artifact of vessel orientation. Given the high cell densities in the RMS, however, the increased blood vessel density could reflect the high metabolic demands of the area. To control for cell density, we compared blood vessel density in the RMS to that in the granule cell layer of the cerebellum. The cell density of granule cells in the cerebellum (3.297×10^6±181,484 cells/mm^3) is significantly higher than all regions of the RMS, even the elbow (2.738×10^6±139,492 cells/mm^3), but the blood vessel density is lower (60% of density in Elbow) (Figure 2J,K). Moreover, within the cerebellum, the density of blood vessels does not differ between the granule cell layer and less dense regions (grey bars in 2J). The high density of blood vessels in the RMS, therefore, is unlikely to be accounted for by the high density of cells.

As can be seen in Figure 2, not every neuroblast is in direct contact with a blood vessel. It does appear, however, that most blood vessels have aligned neuroblasts closely apposed. For each area of the RMS, we quantified the percent length of each longitudinally cut vessel with apposed neuroblasts, and termed this measure linear apposition percentage. Within the SVZ, where there is a recognized association between stem cells and vessels, in what is termed the neurovascular niche, 53.8±5.1% of the length of blood vessels is apposed by neuroblasts. This increases significantly along the course of the RMS, to 61.3±1.5% in the Descent, 77.6±2.4% in the Elbow, 86.1±1.8% at the Entrance, and 83.7%±1.5% in the OB (Figure 2L).

The increased density of blood vessels in the RMS, the fact that they are aligned along the path of migration, and the large percentage of vessel length that is lined by neuroblasts all suggest that the neuroblasts use the vessels as a migratory scaffold. The vessels may also be secreting substances that affect neuronal migration. In most brain regions, astrocytic endfeet wrap the vasculature to create the blood-brain barrier, restricting the exchange of substances between the blood and the brain parenchyma. Given the recognized importance of astrocytes in the RMS, we next asked if astrocytes might be establishing an intermediate apposition that could mediate interactions between endothelial cells and neuroblasts.

We first examined the density and distribution of GFAP-expressing astrocytes along the RMS. Because GFAP stains processes more clearly than cell bodies, and because we were interested in how those processes relate to the migrating neuroblasts and blood vessels, we used area of GFAP staining, rather than cell number, as our measure. Astrocytes have been reported to form tubes around chains of migrating neuroblasts, possibly acting as a physical barrier preventing premature exit from the migratory stream (Lois et al., 1996). As can be seen in Figure 3, at all levels of the RMS, GFAP processes interdigitate with migrating neuroblasts, but do not seem to form a continuous sheath around the full extent of the RMS, as might be expected if they were a physical barrier preventing neuroblasts from prematurely exiting the stream. To quantify this, we measured GFAP density within the RMS, and compared it to GFAP density in the region within 10μm (approximately one cell body diameter) from the edge of DCX staining. In all regions, except within the bulb, GFAP staining was denser within the RMS than around it, suggesting that glial tubes do not form a continuous physical barrier outlining the path of migration. Within the OB, the difference in GFAP density between areas within the RMS and directly surrounding it disappears, possibly reflecting a breakdown in the structure of the RMS as cells break off of chains and migrate radially into the GCL.

We hypothesized that astrocytes might ensheath blood vessels and the neuroblasts along them. When we stained for DCX, PECAM and GFAP, astrocytic processes often separated neuroblasts and vessels. There were instances, however, where there did not appear to be an intervening astrocytic process (Figure 4A-B, arrows and insets). Because GFAP is an intermediate filament protein, and is not expressed in the smallest processes of astrocytes, particularly the endfeet surrounding capillaries (Iadecola and Nedergaard, 2007), we used electron microscopy to further define the relationship between glia, neuroblasts, and blood vessels. As expected, we saw examples of blood vessels in which surrounding pericytes and astrocytes were intermediate between the endothelial cell and the migrating neuroblast (Figure 4C-F). We saw other examples, however, of neuroblasts directly apposed to longitudinally cut vessels, without any intervening astrocytes or pericytes (Figure 4G-J). This latter observation supports our immunohistochemical staining suggesting that migrating neuroblasts can directly contact endothelial cells.

Using GFAP, it is often difficult to distinguish individual astrocytes, so to study the morphology and 3-dimensional orientation of individual astrocytes within the RMS we turned to intracellular dye injections. Using slices from DCX-GFP mice, we injected fluorescent dextran into non-GFP-expressing cells in each region of the RMS, and then made 3-dimensional reconstructions of the labeled astrocytes and neighboring migrating chains. The cell bodies of the astrocytes labeled with dextran often had a somewhat elliptical appearance, with numerous extending astrocytic processes (Figure 5) which were positive for GFAP (Supplemental Figure 1). However, the most striking aspect of astrocyte morphology in the RMS is that the astrocytic branches are aligned with the path of migration; they do not exhibit the typical stellate morphology usually associated with astrocytes. The processes extending from a single cell appear organized into narrow tangentially oriented columns and do not extend radially within or outside of the RMS.

Correspondingly, in coronal slices, where migration would be occurring out of the slice, astrocytes did not hold the dye well, presumably because their processes had been cut during sectioning (data not shown). Individual astrocytic processes could be quite long, and often ran along a chain of neuroblasts. Occasionally, a single astrocyte would have two parallel processes, on either side of a migrating chain (Figure 5B and D, see also Supplemental Figure 2B and D). We also observed astrocytic endfeet along a migrating chain (Figure 5C and Supplemental Figure 2C). The 3-dimensional reconstructions helped uncover the relations among astrocytes and chains of migrating neuroblasts. They not only made clear the parallel alignment of astrocytic processes with often more than one chain (Supplemental Movie M1), but also showed that astrocytes formed grooves that engulfed migrating chains (Supplemental Movie M2) and suggested that astrocytes could simultaneously be in close association with blood vessels (note the concave nucleus indicative of a blood vessel endothelial cell in Supplemental Figure 2B and Supplemental Movie 2), which was confirmed by immunohistochemistry (Supplemental Figure 3).

DISCUSSION

To better understand neuroblast migration, we have studied the architecture of the RMS along its entire rostral-caudal extension in the adult mouse. We divided the RMS into five regions and examined the relationships between migrating neuroblasts, glia, and the vasculature at each location. Throughout, blood vessels are parallel and aligned with the direction of migration in the RMS, and are lined by chains of migrating neuroblasts. Such uniformity in the orientation of blood vessels is not apparent elsewhere in the nervous system. Moreover, the density of blood vessels within the RMS is significantly higher than other areas of brain, including comparably cell-dense areas in the cerebellum. Astrocytes in the RMS have more complex morphologies than previously hypothesized, with long processes aligned parallel to the path of migration. Astrocytes line both vessels and migrating chains and may mediate their interactions, although we also documented examples of direct contact between endothelial cells and neuroblasts.

Cell types in the RMS

The RMS is extremely cell-dense, with over 1.7 million cells/mm^3, and greater than 1.2 million neuroblasts/mm^3. It is most tightly packed at the elbow, as the RMS narrows in the olfactory peduncle. Along the course of the RMS, the proportion of cells that are neuroblasts (DCX^+) increases, but there is no change in the density of glial processes. This likely reflects increasing maturity as cells move rostrally, and as transit-amplifying cells divide to form DCX^+ neuroblasts. Caudal regions of the RMS also contain neural stem cells, which give rise to specific subtypes of olfactory interneurons (Hack et al., 2005; Merkle et al., 2007; Young et al., 2007). The higher percentage of neuroblasts in the rostral areas of the RMS may therefore reflect the absence of these precursor cells.

Relationship of migrating cells to blood vessels

Our results provide compelling evidence that blood vessels provide a migratory scaffold for neuroblasts in the RMS. In contrast to the random orientation of blood vessels in other brain regions, blood vessels within the RMS are aligned parallel to the direction of migration. The density of vessels in the RMS is also significantly higher than in other brain regions. This increased vessel density is not necessitated by the high cell density in the RMS, since an equally cell-dense area, the granule cell layer of the cerebellum, has a lower vessel density. Additionally, there is no difference between blood vessel density in the granule cell layer and in other, less dense, areas of the cerebellum. This suggests that the increased density of blood vessels in the RMS is not a consequence of higher cell density or greater metabolic demand than surrounding tissue.

We further found that chains of migrating neurons are directly aligned along the vessels, apparently migrating along them. In rostral regions of the RMS, over 80% of the length of each vessel is lined by chains of neuroblasts. A recent report has suggested that neuroblasts use blood vessels as a scaffold for radial migration in the OB, when they are no longer migrating in chains (Bovetti et al., 2007). We further propose that throughout the RMS, chains follow blood vessels, and that as they enter the OB individual chains may follow a blood vessel out of the RMS before individual cells turn radially.

Links between the nervous and vascular systems

It has become increasingly clear that there are many links and common signaling mechanisms between the vascular and nervous systems. Many of the same cues influence cell fate decisions, migration, branching, and proliferation in both systems (Carmeliet, 2003). The same growth factors can stimulate both neurogenesis and angiogenesis, during both embryonic development and adulthood (Carmeliet and Tessier-Lavigne, 2005; Klagsbrun and Eichmann, 2005; Ward and Lamanna, 2004). In neurogenic regions in adults, endothelial cells and neural stem cells (NSCs) interact within the neurovascular niche (Tavazoie et al., 2008). Vascular-endothelial growth factor (VEGF) stimulates proliferation of endothelial cells, which then secrete brain-derived neurotrophic factor (BDNF), promoting neurogenesis (Louissaint et al., 2002). VEGF also increases proliferation in the SVZ, and DCX-expressing neuroblasts express the receptor VEGFR2/Flk-1 (Jin et al., 2002). The interactions between NSCs and endothelial cells are bidirectional, with co-culture stimulating self-renewal and neuronal production from NSCs and tube formation and VEGF and BDNF production by endothelial cells (Leventhal et al., 1999; Li et al., 2006; Shen et al., 2004). Our data suggest that as NSCs differentiate into neuroblasts and migrate into the OB, they remain associated with vessels, which influence not only proliferation, but also migration.

Neuroblast migration along blood vessels

Following stroke, neuroblasts migrate from the SVZ to areas of infarct in close association with blood vessels in the hypoxic area (Ohab et al., 2006; Thored et al., 2007; Yamashita et al., 2006). Stroke-induced hypoxia leads to angiogenesis, which may attract or guide neuroblasts from the SVZ (Thored et al., 2007), by vascular production of Ang1 and SDF1 (Ohab et al., 2006). Consistent with VEGF's role in both angiogenesis and neurogenesis, mice that over express VEGF show greater functional recovery and increased neurogenesis in the SVZ and at the ischemic border after infarct (Wang et al., 2007). Transplanted neuronal precursor cells have also been shown to associate with blood vessels (Betarbet et al., 1996; Honda et al., 2007). We show that neuroblasts migrate along blood vessels not just in the injured brain, but under normal conditions along their normal migratory route.

The results from stroke models suggest that angiogenesis attracts neuroblasts from the SVZ, possibly through vascular production of soluble attractive factors. Our results, that neuroblasts are associated with vessels under normal conditions in the RMS, suggest several possibilities. There may be continuous high levels of angiogenesis in the RMS, although why this would occur is not clear. More likely, endothelial cells in the RMS may constitutively secrete attractive factors that are stimulated by hypoxia in other regions. In addition to secreting attractive factors, blood vessels and their basal lamina may act as a physical scaffold for neuroblasts, possibly by interacting with cell surface molecules such as integrins and related molecules that may contribute to cell:cell interactions (Belvindrah et al., 2007; Emsley and Hagg, 2003; Murase and Horwitz, 2002).

Role of glia

Astrocytes play a prominent role in the RMS, surrounding chains of migrating neuroblasts (Alvarez-Buylla and Garcia-Verdugo, 2002) and modulating the microenvironment (Bolteus and Bordey, 2004). Astrocytic endfeet also wrap brain vasculature, contributing to the blood-brain barrier, and are involved in regulating cerebrovascular dynamics, to match blood flow to areas of metabolic demand (Gordon et al., 2007; Iadecola and Nedergaard, 2007). Because in many cases astrocytic processes separate neuroblasts from the endothelial cells, RMS astrocytes may mediate interactions between neuroblasts and endothelial cells. Some neuroblasts are directly apposed to endothelial cells, however, and may receive signals directly, unmediated by astrocytes.

The current model of cellular organization in the RMS involves chains of neurons migrating along each other, ensheathed by glial tubes, without additional scaffolding (Alvarez-Buylla and Garcia-Verdugo, 2002). We do not, however, see evidence of glial processes completely ensheathing the full migratory stream, as might be expected if the glial tubes form a physical barrier restricting neuroblast migration, as has been suggested. Instead, individual astrocytes are highly polarized, with long processes aligned with migrating chains, rather than wrapping around them. These processes also line the dense blood vessels in the area. The vessels and astrocytes may therefore combine to form a complex scaffold for migration, in addition to functioning as modulators of the migratory microenvironment.

During embryonic and postnatal development in other brain regions, neurons migrate along relatively simple glial scaffolds, with one neuron migrating along a single glial process. The RMS is unique in that neurons migrate along each other in chains, without such a simple scaffold. We show here that the vasculature delineates the path of migration from the SVZ into the OB, and may form a scaffold along which chains of neurons migrate. Manipulation of the vasculature may therefore be an important strategy in attempts to re-route neuronal precursors to areas of injury or neurodegeneration.

Supplementary Material

Refer to Web version on PubMed Central for supplementary material.

Acknowledgments

We are grateful to Dr. Angelique Bordey for the DCX-GFP mice and to Dr. Joseph Madri and Sandra Canosa for the PECAM antibody as well as for helpful discussions. We thank Dolores Montoya and Christine Kaliszewski for expert technical assistance, and all members of the Greer lab for helpful discussions and critical reading of the manuscript.

Supported by DC000210, DC006291 and DC006972. MCW was supported by the Yale MSTP Grant GM07205.

References

Alvarez-Buylla A, Garcia-Verdugo JM. Neurogenesis in adult subventricular zone. J Neurosci. 2002; 22(3):629–634. [PubMed: 11826091]

Alvarez-Buylla A, Garcia-Verdugo JM, Tramontin AD. A unified hypothesis on the lineage of neural stem cells. Nat Rev Neurosci. 2001; 2(4):287–293. [PubMed: 11283751]

Alvarez-Buylla A, Lim DA. For the long run: maintaining germinal niches in the adult brain. Neuron. 2004; 41(5):683–686. [PubMed: 15003168]

Anton ES, Ghashghaei HT, Weber JL, McCann C, Fischer TM, Cheung ID, Gassmann M, Messing A, Klein R, Schwab MH, Lloyd KC, Lai C. Receptor tyrosine kinase ErbB4 modulates neuroblast migration and placement in the adult forebrain. Nat Neurosci. 2004; 7(12):1319–1328. [PubMed: 15543145]

Belvindrah R, Hankel S, Walker J, Patton BL, Muller U. Beta1 integrins control the formation of cell chains in the adult rostral migratory stream. J Neurosci. 2007; 27(10):2704–2717. [PubMed: 17344408]

Betarbet R, Zigova T, Bakay RA, Luskin MB. Migration patterns of neonatal subventricular zone progenitor cells transplanted into the neonatal striatum. Cell Transplant. 1996; 5(2):165–178. [PubMed: 8689029]

Bolteus AJ, Bordey A. GABA release and uptake regulate neuronal precursor migration in the postnatal subventricular zone. J Neurosci. 2004; 24(35):7623–7631. [PubMed: 15342728]

Bovetti S, Hsieh YC, Bovolin P, Perroteau I, Kazunori T, Puche AC. Blood vessels form a scaffold for neuroblast migration in the adult olfactory bulb. J Neurosci. 2007; 27(22):5976–5980. [PubMed: 17537968]

Brown JP, Couillard-Despres S, Cooper-Kuhn CM, Winkler J, Aigner L, Kuhn HG. Transient expression of doublecortin during adult neurogenesis. J Comp Neurol. 2003; 467(1):1–10. [PubMed: 14574675]

Carmeliet P. Blood vessels and nerves: common signals, pathways and diseases. Nat Rev Genet. 2003; 4(9):710–720. [PubMed: 12951572]

Carmeliet P, Tessier-Lavigne M. Common mechanisms of nerve and blood vessel wiring. Nature. 2005; 436(7048):193–200. [PubMed: 16015319]

Chazal G, Durbec P, Jankovski A, Rougon G, Cremer H. Consequences of neural cell adhesion molecule deficiency on cell migration in the rostral migratory stream of the mouse. J Neurosci. 2000; 20(4):1446–1457. [PubMed: 10662835]

Doetsch F, Alvarez-Buylla A. Network of tangential pathways for neuronal migration in adult mammalian brain. PNAS. 1996; 93(25):14895–14900. [PubMed: 8962152]

Doetsch F, Caille I, Lim DA, Garcia-Verdugo JM, Alvarez-Buylla A. Subventricular zone astrocytes are neural stem cells in the adult mammalian brain. Cell. 1999; 97(6):703–716. [PubMed: 10380923]

Emsley JG, Hagg T. alpha6beta1 integrin directs migration of neuronal precursors in adult mouse forebrain. Exp Neurol. 2003; 183(2):273–285. [PubMed: 14552869]

Ghashghaei HT, Lai C, Anton ES. Neuronal migration in the adult brain: are we there yet? Nat Rev Neurosci. 2007; 8(2):141–151. [PubMed: 17237805]

Gong S, Zheng C, Doughty ML, Losos K, Didkovsky N, Schambra UB, Nowak NJ, Joyner A, Leblanc G, Hatten ME, Heintz N. A gene expression atlas of the central nervous system based on bacterial artificial chromosomes. Nature. 2003; 425(6961):917–925. [PubMed: 14586460]

Gordon GR, Mulligan SJ, MacVicar BA. Astrocyte control of the cerebrovasculature. Glia. 2007; 55(12):1214–1221. [PubMed: 17659528]

Hack MA, Saghatelyan A, de Chevigny A, Pfeifer A, Ashery-Padan R, Lledo PM, Gotz M. Neuronal fate determinants of adult olfactory bulb neurogenesis. Nat Neurosci. 2005; 8(7):865–872. [PubMed: 15951811]

Honda S, Toda K, Tozuka Y, Yasuzawa S, Iwabuchi K, Tomooka Y. Migration and differentiation of neural cell lines transplanted into mouse brains. Neurosci Res. 2007; 59(2):124–135. [PubMed: 17651850]

Iadecola C, Nedergaard M. Glial regulation of the cerebral microvasculature. Nat Neurosci. 2007; 10(11):1369–1376. [PubMed: 17965657]

Jankovski A, Sotelo C. Subventricular zone-olfactory bulb migratory pathway in the adult mouse: cellular composition and specificity as determined by heterochronic and heterotopic transplantation. J Comp Neurol. 1996; 371(3):376–396. [PubMed: 8842894]

Jin K, Zhu Y, Sun Y, Mao XO, Xie L, Greenberg DA. Vascular endothelial growth factor (VEGF) stimulates neurogenesis in vitro and in vivo. PNAS. 2002; 99(18):11946–11950. [PubMed: 12181492]

Klagsbrun M, Eichmann A. A role for axon guidance receptors and ligands in blood vessel development and tumor angiogenesis. Cytokine Growth Factor Rev. 2005; 16(4-5):535–548. [PubMed: 15979925]

Komitova M, Zhu X, Serwanski DR, Nishiyama A. NG2 cells are distinct from neurogenic cells in the postnatal mouse subventricular zone. J Comp Neurol. 2009; 512(5):702–716. [PubMed: 19058188]

Leventhal C, Rafii S, Rafii D, Shahar A, Goldman SA. Endothelial trophic support of neuronal production and recruitment from the adult mammalian subependyma. Mol Cell Neurosci. 1999; 13(6):450–464. [PubMed: 10383830]

Li Q, Ford MC, Lavik EB, Madri JA. Modeling the neurovascular niche: VEGF- and BDNF-mediated cross-talk between neural stem cells and endothelial cells: an in vitro study. J Neurosci Res. 2006; 84(8):1656–1668. [PubMed: 17061253]

Lois C, Alvarez-Buylla A. Long-distance neuronal migration in the adult mammalian brain. Science. 1994; 264(5162):1145–1148. [PubMed: 8178174]

Lois C, Garcia-Verdugo JM, Alvarez-Buylla A. Chain migration of neuronal precursors. Science. 1996; 271(5251):978–981. [PubMed: 8584933]

Louissaint A Jr. Rao S, Leventhal C, Goldman SA. Coordinated interaction of neurogenesis and angiogenesis in the adult songbird brain. Neuron. 2002; 34(6):945–960. [PubMed: 12086642]

Merkle FT, Mirzadeh Z, Alvarez-Buylla A. Mosaic organization of neural stem cells in the adult brain. Science. 2007; 317(5836):381–384. [PubMed: 17615304]

Murase S, Horwitz AF. Deleted in colorectal carcinoma and differentially expressed integrins mediate the directional migration of neural precursors in the rostral migratory stream. J Neurosci. 2002; 22(9):3568–3579. [PubMed: 11978833]

Ohab JJ, Fleming S, Blesch A, Carmichael ST. A neurovascular niche for neurogenesis after stroke. J Neurosci. 2006; 26(50):13007–13016. [PubMed: 17167090]

Pencea V, Luskin MB. Prenatal development of the rodent rostral migratory stream. J Comp Neurol. 2003; 463(4):402–418. [PubMed: 12836176]

Piali L, Hammel P, Uherek C, Bachmann F, Gisler RH, Dunon D, Imhof BA. CD31/PECAM-1 is a ligand for alpha v beta 3 integrin involved in adhesion of leukocytes to endothelium. J Cell Biol. 1995; 130(2):451–460. [PubMed: 7542249]

Pinter E, Barreuther M, Lu T, Imhof BA, Madri JA. Platelet-endothelial cell adhesion molecule-1 (PECAM-1/CD31) tyrosine phosphorylation state changes during vasculogenesis in the murine conceptus. Am J Pathol. 1997; 150(5):1523–1530. [PubMed: 9137078]

Pinter E, Mahooti S, Wang Y, Imhof BA, Madri JA. Hyperglycemia-induced vasculopathy in the murine vitelline vasculature: correlation with PECAM-1/CD31 tyrosine phosphorylation state. Am J Pathol. 1999; 154(5):1367–1379. [PubMed: 10329590]

Platel JC, Lacar B, Bordey A. GABA and glutamate signaling: homeostatic control of adult forebrain neurogenesis. J Mol Histol. 2007; 38(4):303–311. [PubMed: 17554632]

Shen Q, Goderie SK, Jin L, Karanth N, Sun Y, Abramova N, Vincent P, Pumiglia K, Temple S. Endothelial cells stimulate self-renewal and expand neurogenesis of neural stem cells. Science. 2004; 304(5675):1338–1340. [PubMed: 15060285]

Tavazoie M, Van der Veken L, Silva-Vargas V, Louissaint M, Colonna L, Zaidi B, Garcia-Verdugo JM, Doetsch F. A specialized vascular niche for adult neural stem cells. Cell Stem Cell. 2008; 3(3):279–288. [PubMed: 18786415]

Thored P, Wood J, Arvidsson A, Cammenga J, Kokaia Z, Lindvall O. Long-Term Neuroblast Migration Along Blood Vessels in an Area With Transient Angiogenesis and Increased Vascularization After Stroke. Stroke. 2007

Wang Y, Jin K, Mao XO, Xie L, Banwait S, Marti HH, Greenberg DA. VEGF-overexpressing transgenic mice show enhanced post-ischemic neurogenesis and neuromigration. J Neurosci Res. 2007; 85(4):740–747. [PubMed: 17243175]

Ward NL, Lamanna JC. The neurovascular unit and its growth factors: coordinated response in the vascular and nervous systems. Neurol Res. 2004; 26(8):870–883. [PubMed: 15727271]

Whitman MC, Greer CA. Adult-generated neurons exhibit diverse developmental fates. Dev Neurobiol. 2007a; 67(8):1079–1093. [PubMed: 17565001]

Whitman MC, Greer CA. Synaptic integration of adult-generated olfactory bulb granule cells: basal axodendritic centrifugal input precedes apical dendrodendritic local circuits. J Neurosci. 2007b; 27(37):9951–9961. [PubMed: 17855609]

Wichterle H, Garcia-Verdugo JM, Alvarez-Buylla A. Direct evidence for homotypic, glia-independent neuronal migration. Neuron. 1997; 18(5):779–791. [PubMed: 9182802]

Yamashita T, Ninomiya M, Hernandez Acosta P, Garcia-Verdugo JM, Sunabori T, Sakaguchi M, Adachi K, Kojima T, Hirota Y, Kawase T, Araki N, Abe K, Okano H, Sawamoto K. Subventricular zone-derived neuroblasts migrate and differentiate into mature neurons in the post-stroke adult striatum. J Neurosci. 2006; 26(24):6627–6636. [PubMed: 16775151]

Young KM, Fogarty M, Kessaris N, Richardson WD. Subventricular zone stem cells are heterogeneous with respect to their embryonic origins and neurogenic fates in the adult olfactory bulb. J Neurosci. 2007; 27(31):8286–8296. [PubMed: 17670975]

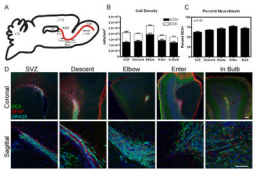

Figure 1. Divisions of the RMS

A: Schematic of a sagittal section of the mouse brain, showing delineations for each region of the RMS. B: Cell density is high throughout the RMS, and increases in the elbow. Black bars represent DCX^+ neuroblasts, and white bars represent DCX^- cells. Overall density and DCX^+ density both increase in the elbow, one-way ANOVA $p<0.05$. C: The proportion of DCX^+ cells increases along the RMS. One-way ANOVA $p<0.05$. Error bars represent SEM. D: Representative images of each region of the RMS. Low-power coronal (top row) and high-power sagittal images (bottom row) of the RMS are shown for each region. Neuroblasts are labeled with DCX (green), glia with GFAP (red) and nuclei with DRAQ5 (blue). Scale bars equal 50μm for each row. Individual color channels are shown in Supplemental Figure 4.

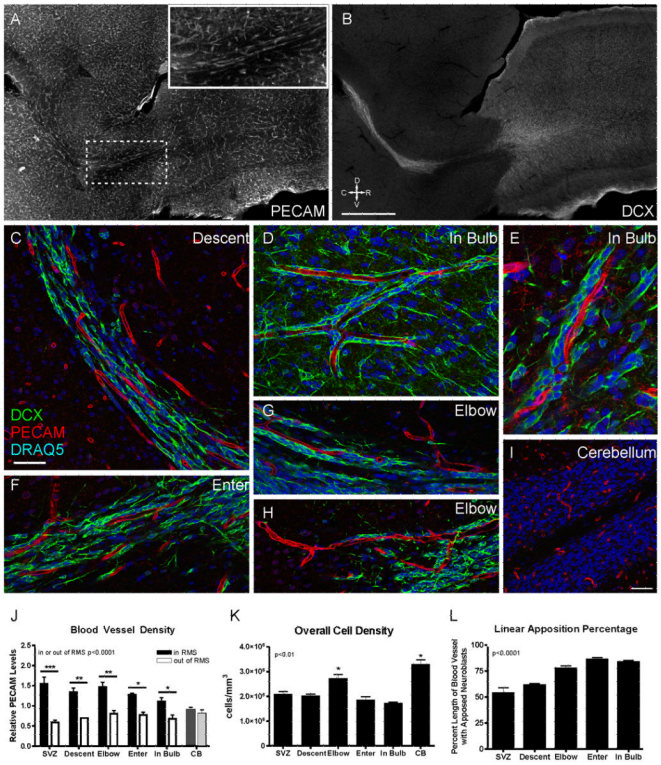

Figure 2. Neuroblasts Align Along Blood Vessels Throughout the RMS

A-B: Sagittal images showing the alignment of blood vessels (A, PECAM) along the migratory path (B, DCX). The inset in A shows the boxed region. Note the longitudinal vessels along the RMS and the random orientation elsewhere. Scale bar in B equals 1mm in A and B. C-E: Sagittal confocal images show the increased density of blood vessels within the RMS, their alignment with the direction of migration, and the apposition of chains of neuroblasts. Neuroblasts are labeled with DCX (green), vessels with PECAM (red) and nuclei with DRAQ5 (blue). Images are from the regions indicated; the cerebellum is included for comparison to an equally cell dense region. Scale bar in C equals 50μm in C,D,F-H, 25μm in E, and 80μm in I. J: Blood vessel density is higher within the RMS (black bars) than in areas outside it (white bars). In the cerebellum, there is no difference in blood vessel density between the most dense areas (dark grey bar) and less dense areas (light grey bar), indicating that high cell density does not explain the increased blood vessel density in the RMS. Two-way ANOVA shows a significant effect of in versus out of RMS ($p<0.0001$), Bonferroni post-tests: *$p<0.05$, **$p<0.01$, ***$p<0.001$ K: Overall cell density in the cerebellum is equal to or greater than density in the RMS. One-way ANOVA, $p<0.0001$ L: Vessels throughout the RMS are lined by chains of neuroblasts. Linear apposition percentage is the percent length of each vessel with apposed neuroblasts, which increases significantly along the RMS. One-way ANOVA, $p<0.0001$. Error bars indicate SEM. D: dorsal; V: ventral; C: caudal; R: rostral. Individual color channels of panels C-I are available in Supplemental Figure 5.

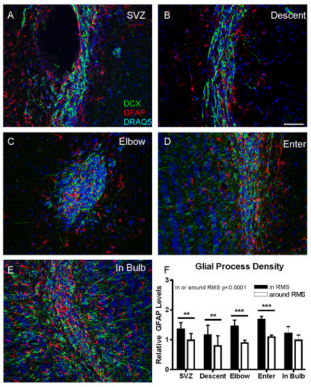

Figure 3. Organization of Glia Along the RMS

A-E: Coronal images of neuroblasts and glia along the RMS. $GFAP^+$ glial processes (red) interdigitate with DCX^+ neuroblasts (green), rather than surround them. Images are from the regions indicated. Scale bar equals 50μm. F: Quantification of GFAP staining within the RMS, and in the area directly around it (within 10μm). In each region, except within the bulb, there is greater GFAP staining in the RMS than directly around it. Two-way ANOVA: $p<0.0001$ for in versus around RMS, Bonferroni posttests: $^{**}p<0.01$, $^{***}p<0.001$. Individual color channels are available in Supplemental Figure 6.

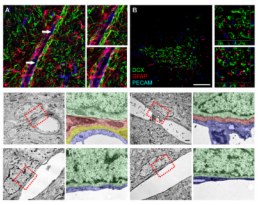

Figure 4. Neuroblasts can directly contact endothelial cells

A-B: Confocal images of DCX^+ neuroblasts (green), along $PECAM^+$ blood vessels (blue), with intervening $GFAP^+$ astrocytic processes (red). A is from a sagittal section in the OB, and B is a coronal section through the Elbow. Arrows in A indicate regions where the neuroblasts appear to directly contact the endothelial cells. Insets are magnifications of these regions. Insets in B are from the boxed regions, and show the z-projections. C-J: Electron micrographs of neuroblasts associated with blood vessels. C-F show examples where an astrocytic process (and a pericyte in C-D) separate the neuroblast and endothelial cell; G-J show examples where the neuroblast and endothelial cell are in direct contact. D, F, H, and J are pseudo-colored magnifications of the boxed areas in C, E, G, and I, respectively. Neuroblasts are colored in green, astrocytes in red, pericytes in yellow and endothelial cells in blue. Scale bar in B equals 50μm in A-B. Scale bar in D equals 1μm in B, D, F, H. Individual color channels of A and B can be seen in supplemental figure 7. Non-colorized electron micrographs can be seen in supplemental figure 8.

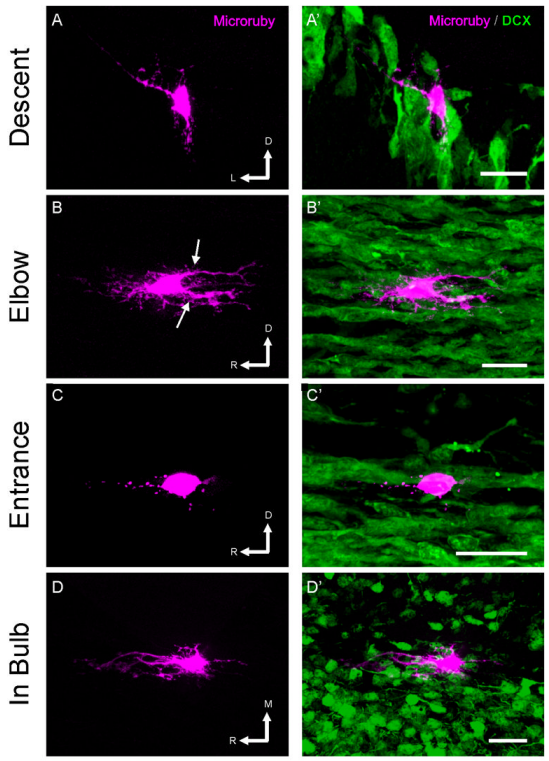

Figure 5. Reconstructions of astrocytes in the RMS

Individual astrocytes in the RMS of DCX-GFP mice were filled by intracellular injection of rhodamine- and biotin- conjugated dextran (magenta) in fixed tissue slices, imaged, and 3D reconstructed. Left panels show volume reconstructions of the astrocyte, and right panels show the relationship of the filled cell to the DCX+ chains of neuroblasts (green). Note the polarity of the astrocytes, with long processes oriented parallel to the direction of migration (arrows). In C, the endfeet of the astrocyte can be seen along a migrating chain. Scale bar: 25 μm. R: rostral; D: dorsal; L: lateral; M: medial. The orientation of tissue sectioning was coronal in A, sagittal in B and C and horizontal in D.